JOM, Vol. 68, No. 10, 2016
DOI: 10.1007/s11837-016-2067-y

Competitive Current Modes for Tunable Ni-Sn Electrodeposition and Their Lithiation/Delithiation Properties

LANCE R. HOFFMAN,[1] CALLUM BREENE,[2] ABDOULAYE DIALLO,[2] RIDWANUR R. CHOWDHURY,[2] and HITOMI MUKAIBO[1,2,3]

1.—Materials Science Program, University of Rochester, Rochester, NY 14627, USA.
2.—Department of Chemical Engineering, University of Rochester, Rochester, NY 14627, USA.
3.—e-mail: hitomi.mukaibo@rochester.edu

Li-ion battery (LIB) anodes with graded composition have the potential to relax interfacial stress and better accommodate the internal stress buildup within the anode during battery operation. A one-dimensional numerical model was developed, where the balance between two competitive current modes (electrokinetic reaction-limited current and diffusion-limited current) defines the deposit composition. The model indicated that the composition of a binary alloy deposit can be varied with overpotential, by decreasing the relative concentration of the more noble element in the plating bath. Indeed, when Ni-Sn alloy was electrodeposited from a Ni^{2+}:Sn^{2+}=50:1 bath, the fraction of Sn in the deposit decreased, from 0.47 to 0.13, with increasing current density. Under this plating condition, Ni-Sn deposits were prepared with uniform, discretized and gradient changes in the deposition current density. Cyclic voltammetry of these samples demonstrated both reversible and irreversible reactions with Li-ion, offering a promising premise for LIB application.

INTRODUCTION

Li-ion batteries (LIBs) are the key energy technology in supporting the demands of hybrid electrical vehicles, electricity consumption and portable electronic devices.[1,2] Lithium-alloying materials are promising alternatives to conventional Li-intercalating anodes, due to their high energy density.[3,4] However, the drastic volume change during battery operation induces stress within the electrode, resulting in significant loss of electrical contact and poor battery performance.[5] Strategies for addressing this challenge includes nanostructural designs and the addition of functional or structural additives.[6]

Recently, a graded-stress nanostructure was proposed as an alternative strategy for improving battery performance.[7,8] This was achieved by co-depositing inactive Cu and active Si with a composition gradient. The graded anode was found to exhibit suppressed delamination and enhanced cycle property, indicating an effective relaxation of the interfacial stress as well as better accommodation of the internal stress.

This paper proposes a versatile, low-cost electrochemical deposition approach to prepare the composition gradient materials for LIB anodes. Sn was chosen over the semiconductive Si because metallic surface is more preferable for continuous electrochemical deposition. Ni was co-deposited with Sn at different molar fractions to act as the buffering agent for reducing lithiation-induced stress. It has been shown that the composition stoichiometry of the Ni-Sn deposit is strongly affected by the plating bath composition and plating current density, due to the competitive contribution of electrokinetic reaction rate and the mass transport rate.[9–14] Electrodeposited Ni-Sn was chosen as the well-studied model anode, but the proposed approach is expected to be applicable to other combinations of elements with different deposition potentials.

Approaches to maximize the control over the deposit's composition are first discussed using a simplified 1D numerical model. The effect of Ni-to-Sn ratio (Ni^{2+}:Sn^{2+}) in the plating bath and the reaction overpotential (η) on the co-deposited Ni and Sn are discussed and experimentally verified through scanning electron microscopy (SEM) and

(Published online August 8, 2016)

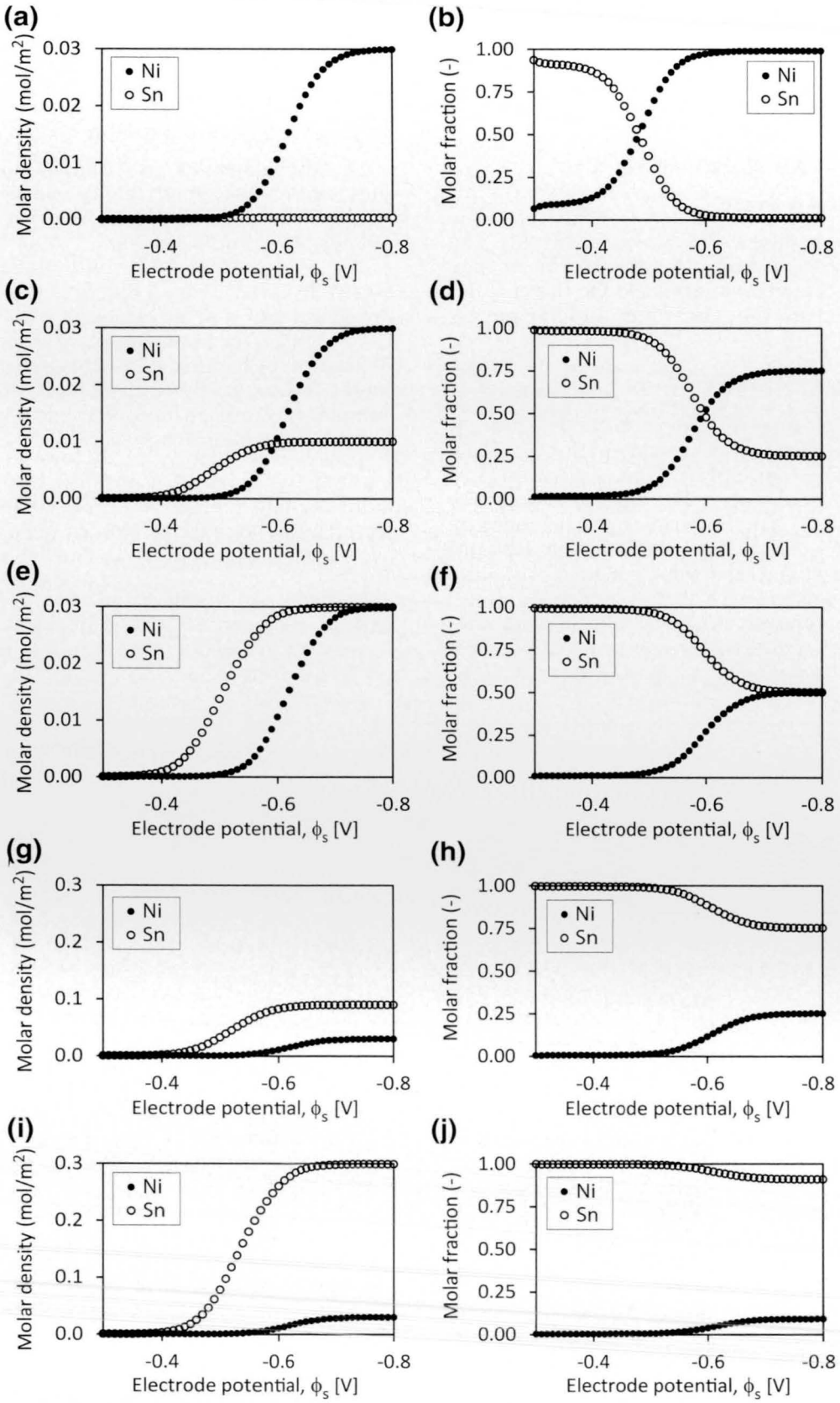

Fig. 1. Effect of electrode potential on Ni and Sn molar density per unit area (left column) and molar fraction of Sn or Ni in the deposit (right column). Ni^{2+}:Sn^{2+} = (a, b) 100:1, (c, d) 3:1, (e, f) 1:1, (g, h) 1:3, and (i, j) 1:10; t = 30 min.

energy dispersive x-ray spectroscopy (EDS). Electrochemical reaction between the prepared Ni-Sn deposits and Li-ions and their potential application for LIBs are investigated through cyclic voltammetry (CV) experiment.

EXPERIMENTAL

1D Numerical Analysis

COMSOL Multiphysics® 5.2 was used with the Electrodeposition module. Details of the model, equations and the parameters used for the calculations are given in the electronic supplementary materials.

Electrochemical Ni-Sn Alloy Deposition

Ni-Sn alloy plating solutions contained 125 μM $NiCl_2 \cdot 6\ H_2O$, variable concentration of $SnCl_2 \cdot 2\ H_2O$, 500 mM $K_4P_2O_7$, 250 mM glycine, and 5 mL L^{-1} NH_4OH in deionized water. The desired ratio of the Ni^{2+} and Sn^{2+} ions (Ni^{2+}:Sn^{2+} ratio) was achieved by varying the $SnCl_2 \cdot 2\ H_2O$ concentration from 1.25 μM to 25.0 μM. Cu substrates were polished with fine steel wool, and washed with acetone and 1 M H_2SO_4. Samples were prepared by galvanostatic electrodeposition on the Cu substrates masked with electrochemical tape, under various current density, j, as specified below. All plating was done at 25°C, with no stirring, using the Princeton Applied Research Versastat 4 potentiostat (unless otherwise specified).

Deposit Characterization

The morphologies and compositions of the samples were examined using Zeiss Auriga SEM equipped with EDS. Ni-Sn films were deposited at j of 50, 10, 1, and 0.1 mA cm^{-2}, and Ni^{2+}:Sn^{2+} ratios of 5:1, 10:1, 20:1, 50:1, and 100:1. The exposed electrode area was 0.32 cm^2. Each sample was deposited for a fixed amount of charge (0.19 C). Care was taken to examine only the center of each deposit, in order to negate any edge effects the mask might induce on the film deposition. Details of CV sample preparation and characterization are given in the supplementary material.

RESULTS AND DISCUSSION

Numerical Analysis: Effect of Overpotential on Deposit Composition

In order to understand the generic trend in deposit composition with applied overpotential (η), a numerical model was studied using arbitrary Ni^{2+}:Sn^{2+} ratios of 100:1, 3:1, 1:1, 1:3, and 1:10.

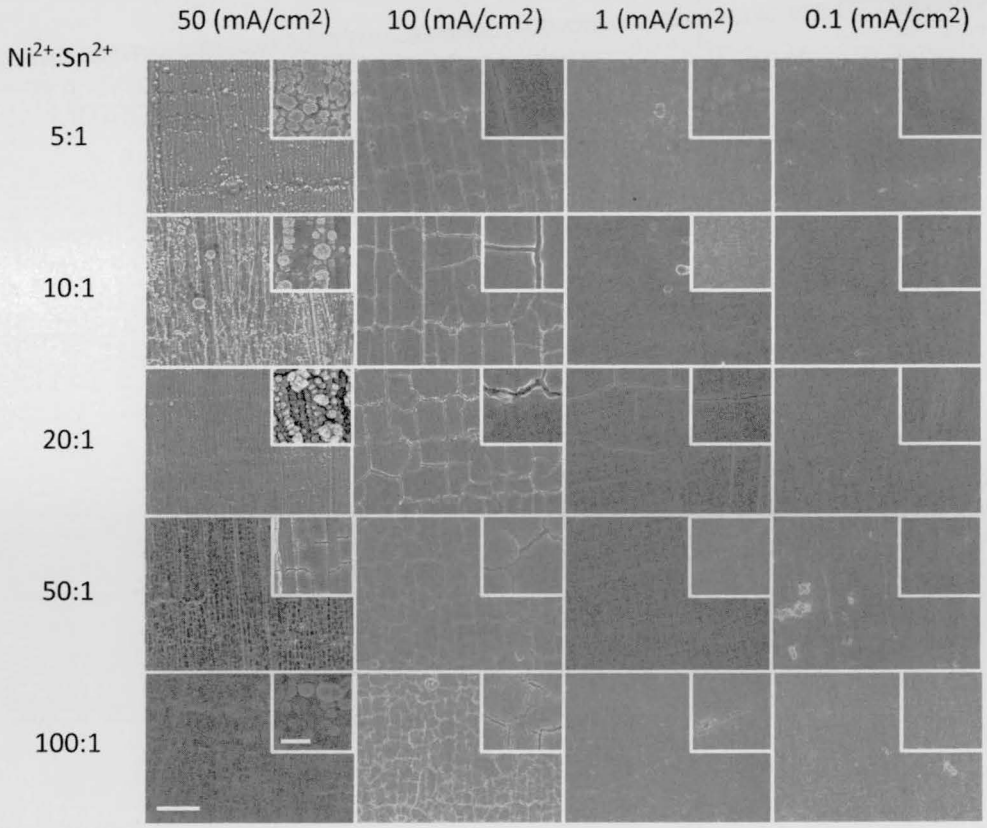

Fig. 2. SEM images of the electrodeposited Ni-Sn alloy surface. The columns and rows indicate different deposition current densities, j, and the Ni^{2+}:Sn^{2+} ratio, respectively. The inset is the same surface imaged at a higher magnification. Scale bars 20 μm and 5 μm for the outer and the inset images, respectively.

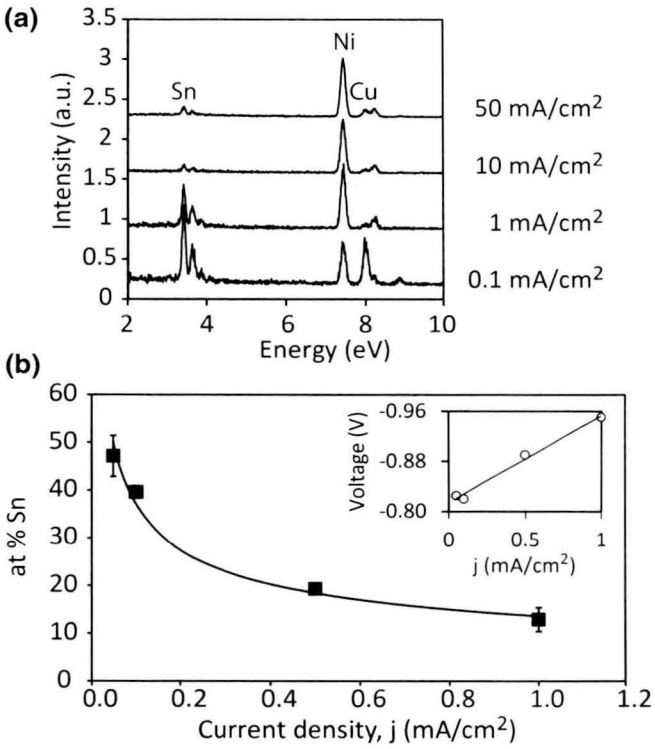

Fig. 3. (a) EDS spectra of the Ni-Sn alloy (from Ni^{2+}:Sn^{2+} = 50:1 bath), deposited at different current densities. (b) EDS analysis of Sn content in the Ni-Sn deposit. The line is a power function that gave the best fit to the data. Inset the steady-state deposition voltage achieved at each current density with a linear line to guide the eye.

Furthermore, the same values were used for the diffusivity, exchange current density, and transfer coefficient of Ni^{2+} and Sn^{2+}, to allow the discussion to focus exclusively on the effect of different standard potential on codeposition. The results of this analysis are summarized in Fig. 1. The quantity of the mass deposited per unity area (mol m^{-2}) is represented by the molar density, σ_m:

$$\sigma_m = -\frac{jt}{zF} \quad (1)$$

where j is the current density, t is the deposition time (30 min), z is the charge of the ions and F is the Faraday constant. From Fig. 1a, little Ni deposits when the applied electrode potential (ϕ_s) is more positive than −0.50 V. The critical ϕ_s where the rise in molar density is confirmed is defined as $\phi_{s,c}$. As the overpotential, η, is increased, the molar density also increases ($-0.50\ V > \phi_s > -0.75\ V$). In this region, larger η decreases the activation energy for metal deposition, increasing cathodic current, and consequently, increasing deposition quantity (Eq. 1). As η is even further increased ($-0.75 > \phi_s$), the molar density becomes independent of ϕ_s. Here, the current is limited by the mass transport of Ni^{2+} to the electrode surface. The critical ϕ_s where diffusion dominates the kinetics is defined as $\phi_{s,d}$.

At low Sn concentration in the electrolyte (Fig. 1a, Ni^{2+}:Sn^{2+} = 100:1), the changes in the amount of Sn deposit with ϕ_s are negligible compared to that of Ni deposition. As the Sn concentration is increased to Ni^{2+}:Sn^{2+} = 3:1 (Fig. 1c), $\phi_{s,c}$ of around −0.40 V is confirmed. The higher $\phi_{s,c}$ for Sn compared to that of Ni is a consequence of the Sn being more noble than Ni. Since the diffusion-limited current is proportional to the bulk concentration (see supplementary material for details), the molar density of Sn is also confirmed to increase linearly with increasing Sn concentration.

The right column of Fig. 1 shows the change in molar fraction of Ni and Sn at various Ni^{2+}:Sn^{2+} ratios. At low η, the molar fraction is defined by the differences in the electrokinetic reaction rate. The more noble Sn deposits much faster than Ni, and hence the fraction of Sn is higher than Ni. The Sn fraction under this condition increases with increasing Sn concentration in the electrolyte. The molar fraction of Ni can be further suppressed by applying lower ϕ_s, or choosing another element that is more noble than Sn. As η increases, the Ni deposition rate increases and starts to gradually take over the molar fraction. The fraction of Ni becomes close to unity under diffusion-limited conditions at low Sn concentration conditions (Fig. 1b). The range of molar fraction decreases as Sn concentration increases (Fig. 1d, f, h, and j).

It is important to note that, in practice, the effect of H_2 evolution reaction (HER) is substantial, and the electrodeposition kinetics will be strongly influenced by issues such as changes in pH and ion complex formation.[15] The convective effect of H_2 bubble formation at the electrode and formation of metal hydroxides are also issues that are not considered here. For in-depth discussions on the numerical analysis of Ni-based alloy deposition considering these interdependent issues are referred to the seminal work by Hessami and Tobias.[16]

Surface Morphology

Figure 2 is a summary of SEM images of Ni-Sn thin films deposited under various Ni^{2+}:Sn^{2+} ratios (i.e. in the electrolyte) and current densities (j). At the highest j examined (50 mA cm^{-2}), the films had the tendency to exhibit nodular (or cauliflower-type) growth. This trend is consistent with what has been previously reported.[10,11,14,17,18] It is interesting to note, however, that nodular growth seemed less prominent at the highest j for Ni^{2+}:Sn^{2+} = 50:1 sample. When j was decreased to 10 mA cm^{-2}, all the Ni^{2+}:Sn^{2+} ratio samples exhibited high density of cracks, and less nodular growth. Such crack formation has been attributed to the internal tensile

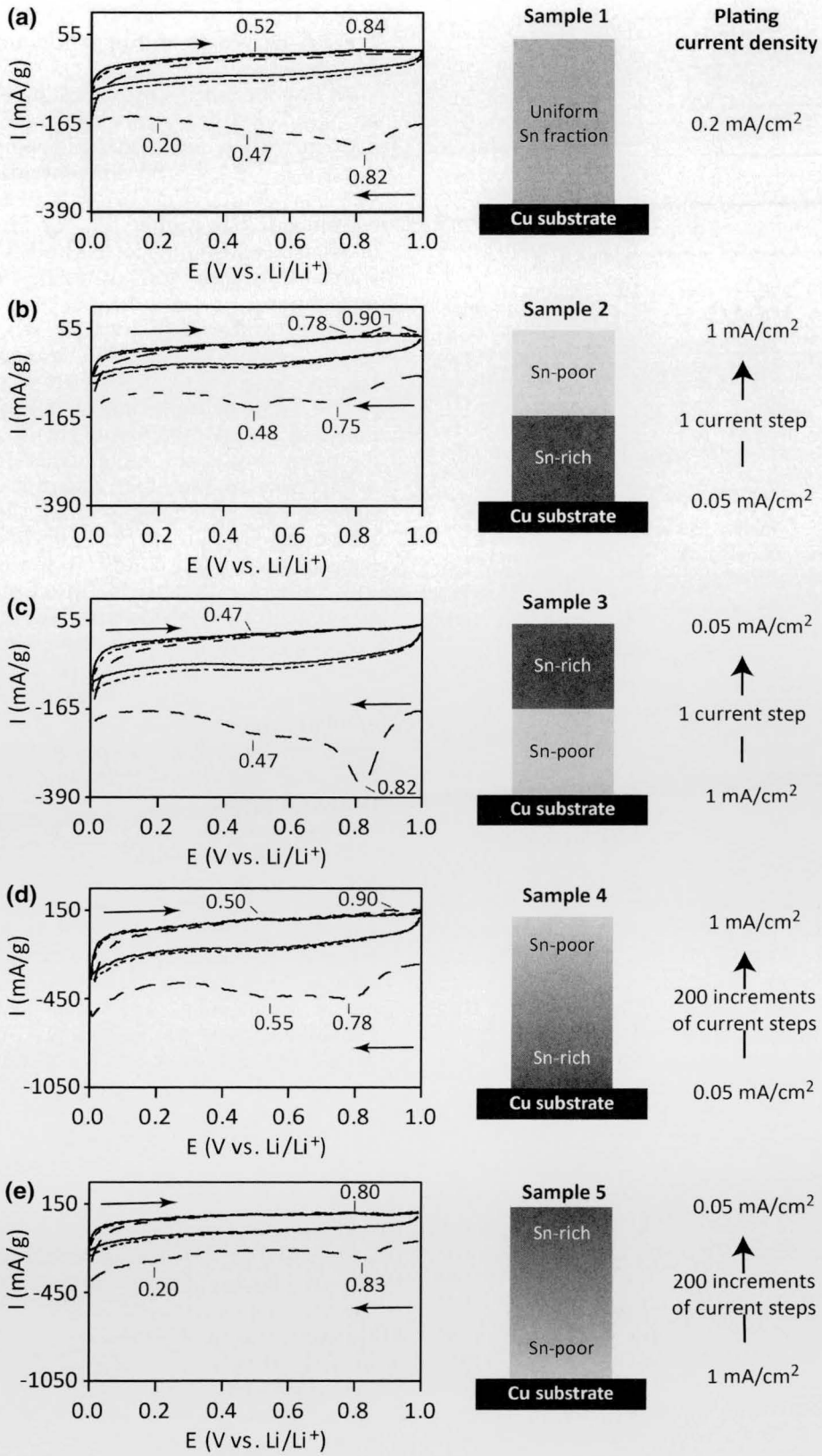

Fig. 4. CVs of (a) uniform sample, (b) discretized sample, Sn-rich on top, (c) discretized sample, Ni-rich on top, (d), gradient sample, Sn-rich on top and (e) gradient sample, Ni rich on top. The arrows in each figure indicate the direction of the scan. Long dashed line 1st cycle, short dashed line 2nd cycle, solid line 3rd cycle. The schemes on the right illustrate the deposition strategy applied for each sample.

stresses that build up during the electrodeposition, caused by impurities, pores and other irregularities within the deposit.[15,19] Both the cracking and the nodular growth were sufficiently suppressed when the deposition occurred at or below 1 mA cm^{-2}.

Based on these trends, j below 1 mA cm^{-2} was chosen to yield deposits with little nodular growth and cracks. Furthermore, the effects of H_2 evolution are assumed to be negligible under this low current density condition.[20] A Ni^{2+}:Sn^{2+} ratio of 50:1 was chosen due to its highest variance in composition at current densities below 1 mA cm^{-2} (see supplementary material).

EDS Analysis

Figure 3a shows the EDS spectra of samples plated from the Ni^{2+}:Sn^{2+} = 50:1 plating bath at different j. A more intense signal for Sn is detected as j decreases. This trend is given quantitatively in Fig. 3b. As shown in the inset, j is linearly related to the deposition voltage, and is a measure of the applied overpotential. Figure 3 demonstrates a decrease in at.% Sn, from 47 at.% Sn to 13 at.% Sn, with increasing overpotential. It is interesting to note that, according to Jović et al.[20] the dominant form of Sn and Ni in the pyrophosphate-plating bath are $[Sn(P_2O_7)_2]^{6-}$, $[Ni(P_2O_7)_2]^{6-}$, and $[Ni(Gly)_3]^-$ complexes. The equilibrium potentials given for the depositions of Sn and Ni from these complexes are −0.845 V and −0.728 V, respectively, which makes the Ni complex more noble than the Sn complex. The discrepancy is attributed to the very high overpotential needed for Ni deposition.[21] As a result, the experimental data followed the trend predicted in our numerical model (Fig. 1a and b)—i.e. the composition of Sn increases with higher overpotential.

The data in Fig. 3b were fitted to a power function with least-squares fitting (R^2 = 0.99):

$$f_{Sn} = 0.136j^{-0.42} \quad (2)$$

where f_{Sn} is the atomic fraction of Sn in the deposit, and j is the current density (mA cm^{-2}). This empirical relationship was used to define j as a function of plating time for the gradient samples in the CV studies discussed below.

Cyclic Voltammetry

Figure 4 shows the CV of the prepared samples, along with schematics to describe the plating strategies used for each sample (numbered 1–5). Cyclic voltammetry was used to study the activity of each sample to lithiation/delithiation reaction. It is quite remarkable that all the samples exhibited some degree of activity, despite the expected low fraction of the total active component (27 at.% Sn). In sample 1, the initial anodic peak and the plateau confirmed at 0.20 V and 0.47 V versus Li/Li^+ decayed by 31% and 43%, respectively, in the second cycle (Fig. 4a). This may be due to the solid–electrolyte interface (SEI) film formation that forms a resistive layer on the electrode surface.[22] SEI that forms during charging (lithiation) is also known for inducing high surface resistance that decreases succeeding discharge (delithiation) capacity, as observed in Fig. 4. On the other hand, the peak at 0.82 V versus Li/Li^+ became indistinguishable in the succeeding cycles, indicative of an irreversible reaction. A similar irreversible peak was confirmed from samples 3 and 5 (Fig. 4c and e). The peak of ~0.82 V versus Li/Li^+ is below the potential reported for SEI formation, and hence this reaction may be attributed to the "conditioning" of the Ni-Sn deposit as it is subjected to the reaction with the Li-ion for the first time.[23] An irreversible peak was also observed for samples 2 and 4 at a lower potential of ~0.75 V versus Li/Li^+ (Fig. 4b and d), which may suggest a higher overpotential for the initial lithiation compared to samples 1, 3, and 5. Characteristic peaks for the lithiation of Sn crystallites were not confirmed, indicating that Sn is either forming an alloy with Ni, or is present within the Ni structure as a solid solution.[11,13]

It is interesting to note that the graded sample 5 (Sn-rich top) exhibits a smaller current than the discretized sample 3 (Sn-rich top), while the graded sample 4 (Sn-poor top) exhibited a larger current than the discretized sample 2 (Sn-poor top). Sample 5 was also unique in that no plateau was observed at 0.47 V versus Li/Li^+. Analyses of the Sn fraction along the thickness of the deposit and the crystallographic structure of these samples are currently underway to assess the differences observed between these samples. Long-term cycling performance and differences in the electrokinetic parameters will also be analyzed to obtain a more comprehensive understanding of the properties of electrochemically-prepared graded samples as LIB anodes.

CONCLUSION

Electrochemical deposition was sought as a promising approach for fabricating gradient LIB anodes. Numerical analysis demonstrated that there is a range of overpotential that can continuously vary the deposit composition, and that a low concentration of the more noble element in the plating bath is the key to achieve a large variance in deposit composition. Electrochemical deposition of thin-film Ni-Sn alloy under different overpotential and Ni^{2+}:Sn^{2+} ratios (in the plating bath) was conducted to confirm this trend. SEM images demonstrated that surface morphology was relatively independent of the Ni^{2+}:Sn^{2+} in the plating bath, while higher current densities resulted in substantial nodular growth or cracking. EDS analysis indicated that the fraction of Sn in the deposit decreased following a power function, from 0.47 to 0.13, with increasing deposition current. CV

demonstrated both reversible and irreversible reactions of Li-ions with the Ni-Sn deposits, offering a promising preliminary overview of the potential application of these materials as LIB anodes.

ACKNOWLEDGEMENT

The research has been conducted under the financial support from the Department of Chemical Engineering at the University of Rochester.

ELECTRONIC SUPPLEMENTARY MATERIAL

The online version of this article (doi:10.1007/s11837-016-2067-y) contains supplementary material, which is available to authorized users.

REFERENCES

1. V. Etacheri, R. Marom, R. Elazari, G. Salitra, and D. Aurbach, *Energy Environ. Sci.* 4, 3243 (2011).
2. P.G. Bruce, B. Scrosati, and J.-M. Tarascon, *Angew. Chem. Int. Ed.* 47, 2930 (2008).
3. W.J. Zhang, *J. Power Sources* 196, 13 (2011).
4. M. Winter and J.O. Besenhard, *Electrochim. Acta* 45, 31 (1999).
5. A. Mukhopadhyay and B.W. Sheldon, *Prog. Mater Sci.* 63, 58 (2014).
6. M.N. Obrovac and V.L. Chevrier, *Chem. Rev.* 114, 11444 (2014).
7. Y. He, J. Fan, and Y. Zhao, *Cryst. Growth Des.* 10, 4954 (2010).
8. B.D. Polat, O.L. Eryilmaz, O. Keles, A. Erdemir, and K. Amine, *Thin Solid Films* 596, 190 (2015).
9. S.D. Beattie and J.R. Dahn, *J. Electrochem. Soc.* 150, C457 (2003).
10. H. Yamashita, T. Yamamura, and K. Yoshimoto, *J. Electrochem. Soc.* 140, 2238 (1993).
11. V.D. Jović, U. Lačnjevac, B.M. Jović, L. Karanović, and N.V. Krstajić, *Int. J. Hydrogen Energy* 37, 17882 (2012).
12. H. Zhang, T. Shi, D.J. Wetzel, R.G. Nuzzo, and P.V. Braun, *Adv. Mater.* 28, 742 (2016).
13. H. Mukaibo, T. Sumi, T. Yokoshima, T. Momma, and T. Osaka, *Electrochem. Solid-State Lett.* 6, A218 (2003).
14. J. Hassoun, S. Panero, and B. Scrosati, *J. Power Sources* 160, 1336 (2006).
15. M. Paunovic and M. Schlessinger, *Fundamentals of Electrochemical Deposition* (Hoboken: Wiley, 1998), p. 211.
16. S. Hessami and C.W. Tobias, *J. Electrochem. Soc.* 136, 3611 (1989).
17. B.M. Jović, U.Č. Lačnjevac, V.D. Jović, and N.V. Krstajić, *J. Electroanal. Chem.* 754, 100 (2015).
18. Y. Zhu, X. Zhang, J. Song, W. Wang, F. Yue, and Q. Ma, *Appl. Catal. A* 500, 51 (2015).
19. H. Jiménez, L. Gil, M.H. Staia, and E.S. Puchi-Cabrera, *Surf. Coat. Technol.* 202, 2072 (2008).
20. U. Lačnjevac, B.M. Jović, and V.D. Jović, *J. Electrochem. Soc.* 159, D310 (2012).
21. V.D. Jović and N. Tošić, *J. Electroanal. Chem.* 441, 69 (1998).
22. J.-T. Li, J. Swiatowska, V. Maurice, A. Seyeux, L. Huang, S.-G. Sun, and P. Marcus, *J. Phys. Chem. C* 115, 7012 (2011).
23. H. Mukaibo, T. Momma, M. Mohamedi, and T. Osaka, *J. Electrochem. Soc.* 152, A560 (2005).